Available online at www.sciencedirect.com

jmr&t Journal of Materials Research and Technology

https://www.journals.elsevier.com/journal-of-materials-research-and-technology

Original Article

Twin boundary-dislocation interactions in nanocrystalline Cu-30% Zn alloys prepared by high pressure torsion

*Xuzhou Gao, Liangjuan Dai, Yonghao Zhao**

Nano and Heterogeneous Materials Center, School of Materials Science and Engineering, Nanjing University of Science and Technology, Nanjing 210094, China

ARTICLE INFO

Article history:
Received 28 February 2020
Accepted 12 August 2020
Available online 2 September 2020

Keywords:
Nanocrystalline Cu-30% Zn
High pressure torsion
Dislocation-twin boundary interaction
Shockley partial dislocation
Frank partial dislocation

ABSTRACT

Preexisting twin boundaries (TBs) and deformation twinning have been reported to significantly improve the strength and ductility of nanocrystalline and ultrafine-grained face-centered cubic (FCC) metals and alloys by interaction between gliding dislocations and TBs. Here, we prepared nanocrystalline Cu-30% Zn alloy with an average size of 80 nm and characterized TB-dislocation interactions by high resolution transmission electron microscopy. Our observations show that the TBs with one or multiple (1 1 1) atomic layer steps were formed either by Shockley partial dislocations slipping along TBs or by reversible reaction between unit dislocations and TBs with the help of sessile Frank partial dislocation dissociation. Moreover, dislocation accumulation at the end of twin lamellae form an asymmetric tilt grain boundary in the matrix and prevent twin propagation. Our findings provide insight into understanding TB migration and strengthening mechanisms in highly twinned FCC metals and alloys.

1. Introduction

Strength and ductility are two of the most important mechanical properties of structural materials. Nanocrystalline (NC, <100 nm) and ultrafine-grained (UFG, <1 μm) materials have been revealed to exhibit significantly higher yield strength than their coarse-grained (CG) counterparts due to the Hall-Petch effect [1,2]. However, the high yield strength is usually achieved at the expense of ductility, and this can be exacerbated in NC and UFG metals because of grain dimensional limitations imposed on the generation and storage of dislocations in grain interiors [1,2]. The poor ductility of the NC and UFG metals has been a major issue limiting their potential structural applications. Many strategies have been proposed to enhance the ductility of NC and UFG metals, including nanoscale second-phase precipitates [3,4], heterogeneous phase interface/grain boundaries (GBs) [5], bi-modal or multi-modal microstructures [6], low stacking fault energy (SFE) [7]. In addition, preexisting twin boundaries (TBs) and deformation twinning [8–11] have been reported to significantly affect the mechanical properties of NC and UFG face-centered cubic (FCC) metals and alloys. Previous experiments [8–11] and molecular dynamics (MD) simulations [12,13] have revealed that nano-scale twins can significantly strengthen metals and alloys while retaining considerable plasticity and work hardening, because TBs usually act as effective barriers for

* *Corresponding author.*
E-mail: yhzhao@njust.edu.cn (Y. Zhao).

https://doi.org/10.1016/j.jmrt.2020.08.060

dislocation motion especially for dislocations with slip planes not parallel to the TBs [9].

According to the literature, dislocation-TB interactions can be affected by multiple parameters complexly, including applied/local stress with respect of the TB [14–16], structure of the TB [17–19] (coherent TB (CTB) or incoherent TB (ITB)), type of incoming dislocation (partial or unit dislocation, screw or non-screw dislocation) [20–22] and twin thickness [12,23,24]. Compression experiments on highly oriented nano-twinned Cu along different directions, illustrated the strong correlation between active slip systems and the direction of applied stress revealing hard and soft model of TB-dislocation interactions [25]. Unit dislocations usually dissociate at the TB to form a partial dislocation slipping along the TB resulting in a de-twinning process. By *in-situ* nano-indentation studies on an epitaxially grown nano-twinned Cu foil, Wang et al. revealed a de-twinning mechanism through a collective glide of the twinning dislocations (i.e. Shockley partial dislocations) [26,27]. Similar results have also been reported in the NC Cu-25% Ni alloy [28] and DP3W duplex stainless steel [29]. In addition, the studies based on MD simulations in Cu, Al and Ni revealed that cross-slip into the twinning plane also induces the twin growth or de-twinning by forming a sessile stair-rod dislocation at TBs and transmission of a dislocation across the TBs as well as twin locks [20,30]. Further inspection of the literature [14–30] indicates that investigations on the dislocation-TB interactions have been focused on metals and alloys with intermediate or high SFEs, while those studies on alloys with extremely low SFE are quite seldom.

In this work, a Cu-30% Zn alloy with extremely low SFE (7 mJ m^{-2}) was selected as a model material. High pressure torsion (HPT) was employed to produce nanocrystalline grains. A large data set was created by extensive high-resolution transmission electron microscopy (HRTEM) analyses in tens of grains with deformation twins in order to reveal the atomic structure of GBs and TBs and the interaction between the glide dislocations and TBs, as well as the mechanism of TB migration.

2. Materials and methods

Cu-30% Zn disks with a thickness of 1.2 mm and a diameter of 10 mm were processed via HPT for 5 revolutions at room temperature under an imposed pressure of 6 GPa and a rotational speed of 1 rpm. The samples were processed under quasi-constrained HPT where each disk was compressed between anvils resulting in a slight flow of material out the disk periphery during the torsion. Specimens for TEM and HRTEM investigations were taken from regions at a distance of 1.5 mm from the disk edge. Thinning was prepared using mechanical grinding followed by ion milling at liquid nitrogen temperature. TEM observations were conducted in an FEI-Tecnai G^2 20 S-TWIN microscope operated at 200 kV. HRTEM was conducted in a Titan G^2 60-300 operated at 300 kV.

3. Results and discussion

3.1. *Grain boundaries*

Fig. 1 illustrates bright- and dark-field TEM images of the HPT-processed Cu-30% Zn alloy. Homogeneously distributed equiaxed nanograins and ultrafine grains with a size ranging from 5 to 160 nm and an average size of 80 nm can be observed. Most grains contain planar structural features, which will be proved as nanotwins and stacking faults (SFs) by following HRTEM analyses. The corresponding selected area electron diffraction (SAED) patterns show relatively continuous rings indicating no obvious preferential grain orientations in the HPT-processed Cu-30% Zn alloy. These results are consistent with our former investigations [31].

Compared with CG metals in which conventional dislocation slip dominates plastic deformation, the high density of GBs in NC and UFG metals have been reported to mediate plasticity through GB sliding [32–34], grain rotation [35–37], stress-driven GB migration [38,39], GB diffusion [40,41], emission of partial dislocations from GBs [42,43] and deformation

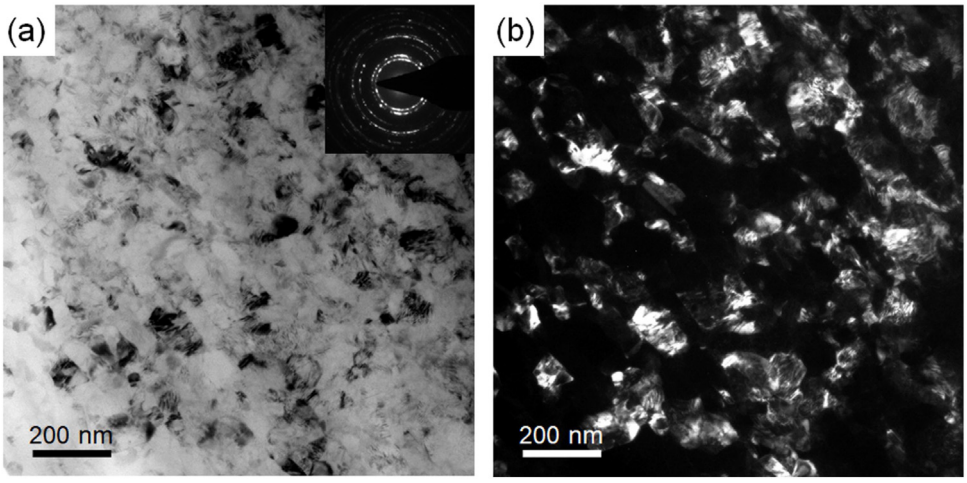

Fig. 1 – Bright- (a) and dark-field (b) TEM images of the HPT-processed Cu-30% Zn alloy, respectively.

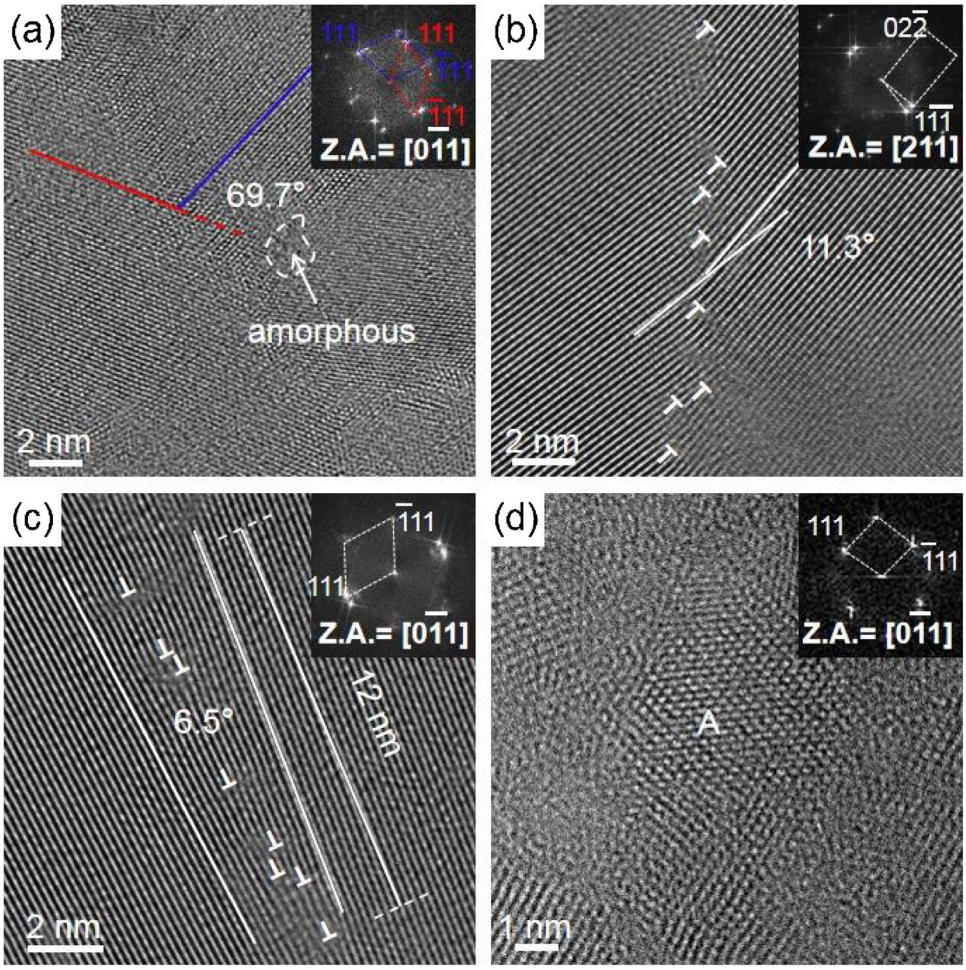

Fig. 2 – HRTEM images of different GBs in the HPT-processed Cu-30% Zn alloy. Insets are the corresponding Filtered Fourier transformation (FFT) patterns. (a) Curved 69.7° HAGB; (b) Curved 11.3° LAGB; (c) 6.5° non-equilibrium LAGB; (d) GB surrounding nano-grain A.

twinning [44]. Therefore, the GB characteristics of the HPT-processed Cu-30% Zn alloy are particularly important. Fig. 2a demonstrates a curved 69.7° high-angle GB (HAGB) and a nanoscale amorphous domain (marked by white dotted line and arrow) was found neighbouring the GB. Our previous investigation on HPT-processed Cu-30% Zn alloy also showed that local amorphization transformation occurs at TBs and extends into the grain interior finally forming curved amorphous GBs [45]. Moreover, high density of dislocations are found to accompany the amorphous embryos [45]. Early theoretical modelling suggested that dislocation accumulation could cause significant elastic strain and stress, resulting in the nucleation of an amorphous structure at dislocation cores [46]. MD simulations [47,48] also revealed that crystalline defects can directly lead to atomic disorder and lattice strain, softening the elastic modulus and destroying the crystallinity. Similar local amorphization caused by dislocation accumulation was also observed in NiTi alloys [49,50], CuZrTi alloy [51], Al alloy [52], and Mg alloy [53], processed by severe plastic deformation.

Besides HAGBs, a high density of low-angle GBs (LAGBs) were also found in the UFG/NC Cu-30% Zn alloy. Fig. 2b displays a paradigmatic 11.3° LAGB, formed by dislocations (marked by white "⊥"). In addition, non-equilibrium GBs were found as important feature of the NC Cu-30% Zn alloy. Fig. 2c shows a 6.5° LAGB containing eight dislocations (marked by the white "⊥") with a length of 12 nm. According to the theory of a equilibrium symmetric tilt GB [54], the average dislocation spacing L is given by the tilt angle θ and the Burgers vector b according to:

$$\frac{b}{L} = 2\sin\frac{\theta}{2} \tag{1}$$

In the Cu-30% Zn alloy, $b = 0.261$ nm for 1/2<1 1 0> dislocations, $\theta = 6.5°$, L was then calculated as 2.3 nm, larger than the measured value of 1.7 nm in Fig. 2c. This result indicates that the GB contains more dislocations than the conventional equilibrium GB, i.e., the LAGB in Fig. 2c is non-equilibrium. Different from the ultrafine grains, the nanograins in the HPT processed Cu-30% Zn alloys are found to be free of dislocations, as shown in Fig. 2d. When the grain size becomes less than a critical grain size, dislocation activity is suppressed in such fine grains [31].

The above results suggest that most GBs of the HPT-processed Cu-30% Zn alloy either contain nanoscale amorphous zone or a massive accumulation of dislocations (non-equilibrium GBs). The dislocation density on the UFG GBs can reach 1.9×10^{16} m^{-2}, while only a few or no dislocations was found in the nanograins.

3.2. TB migration via slip of partial dislocations

Micro-twins are found in most UFG grains, indicating twinning is an important grain refinement mechanisms in the Cu-30% Zn alloy due to its extremely low SFE. According to previous studies, deformation twins in the UFG and NC materials can be formed by continuous emission of partial dislocations from GBs [44]. Moreover, slip of partial dislocations along TBs leads to TB migration [44].

Fig. 3 shows a HRTEM image along [0 −1 1] zone axis of the HPT processed Cu-30% Zn alloy and corresponding inverse filtered Fourier transformation (IFFT) image (Fig. 3c and d). In Fig. 3a a long straight lamella with a thickness of about 3.5 nm is found in a grain. The FFT pattern of the inset reveals a twin relationship with the matrix. Further IFFT analysis of the twin lamella discovered several SFs (marked with white arrows) and unit dislocations (marked with white "⊥") in the twin lamella. Moreover, two steps on the (1 1 1) plane are observed on the upper TB and each step only has a height of one (1 1 1) atomic layer. In order to analyze the formation mechanisms of the (1 1 1) steps via dislocation slip, a Frank circuit (classical method for analyzing dislocations on TBs) was conducted around the step, as shown in Fig. 3b. The Frank circuit reveals a Shockley partial dislocation with a Burgers vector of 1/6[−2 1 1], indicating that the step of one atomic layer height was caused by glide of a Shockley partial dislocation. When the slip direction of the Shockley partial dislocation is consistent with the twinning direction, the TB extends into the matrix accompanying with thickness increase of the twin lamellae [55]. Conversely, movement of the Shockley partial dislocation in opposite direction causes a de-twinning process [55].

Fig. 4 reveals similar results observed in another grain of the HPT processed Cu-30% Zn alloy. Four twin lamella (marked as I, II, III and IV, respectively) with different thicknesses are found within the grain, accompanying atomic steps on the (1 1 1) plane. Magnification of both ends of the micro-twin IV (Fig. 4b and c) reveals a three atomic layers thickness on one end (Fig. 4b) and a Shockley partial dislocation, i.e. SF (marked by white arrow), on the other end (Fig. 4c). The partial dislocation slipped from left to right and stopped inside the grain due to insufficient driving force, by leaving behind a SF in the matrix and a step on the twin lamella.

In-situ TEM observations and MD simulations of a nano-twinned Cu, revealed that twinning and de-twinning with zero net macrostrain can be accomplished via the collective glide of {1 1 2} ITBs [26,27,56–58]. The ITBs were described as a set of Shockley partial dislocations with a repeatable sequence of b_1 (1/6[11−2]): b_2 (1/6[−2 1 1]): b_3 (1/6[1–21]) on the (1 1 1) twin planes, and the net Burgers vector of the three partial dislocations in one unit equals zero. An et al. [28] reported that, under shear stress b_1 will slip ahead smoothly due to its low Peierls barrier, while the paired partials b_2 and b_3 hardly move due to the attractive force from their opposite screw components leading to a non-equilibrium state of the ITB. The resulting SF and the interactions among the three partials will pull the paired partials b_2 and b_3 to approach b_1 until the equilibrium state is achieved again [26]. The repeated alteration between non-equilibrium and equilibrium states, prompts the migration of the ITB and subsequently the growth of the deformation twin [57].

3.3. TB migration via interaction with a unit dislocation

Except for the partial dislocation slip along TBs, interaction of unit dislocations with TB is another important TB migration mechanism, as shown in Fig. 5a. In order to characterize the TB-dislocation interaction, a double Thompson tetrahedron was employed, as illustrated in Fig. 5b. The top Thompson tetrahedron above the ABC (1 1 1) twin boundary represents matrix slip systems, while the bottom tetrahedron represents twin slip systems. The Burgers vector of this dislocation was measured as 0.208 nm, and approaches the theoretical value (0.213 nm) of Frank partial dislocation in the Cu-30% Zn alloy, suggesting a pure Frank partial dislocation. The formation mechanisms of a Frank partial at TBs could be revealed by the following dislocation-TB reactions. When a unit dislocation with Burgers vector of $D'B$ (1/2 [0 1 1]) on AD′B (−1 −1 1) plane interacts with the TB ABC (1 1 1), the unit dislocation dissociates into a Frank partial $D'\delta$ (1/3[1 1 1]) and a Shockley partial δB (1/6[−2 1 1]). The sessile Frank partial $D'\delta$ stays on the TB, because the Burgers vector (1/3[1 1 1]) is not on the conventional close-packed {1 1 1} slip planes, while the Shockley partial δB (1/6[−2 1 1]) slips along the TB, forming a TB step with one (1 1 1) atomic layer. These dislocations destroy the coherency of the TB [59,60], and produce local strain fields and a dragging force to dislocation glide [60]. Therefore, the TB step is pinned by the sessile Frank dislocation and contributes to the strengthening effect [27].

Except for the above TB step with one atomic layer, a more complicated TB migration mechanism caused by the interaction between unit dislocation and TB is revealed in Fig. 6. A TB step with two atomic layers is observed in Fig. 6b. A Frank partial marked with white "⊥" is found on the TB step by conducting the Frank circuit analysis. This result indicates that the TB step with two (1 1 1) atomic layers can be formed by the interaction between the external unit dislocation and the TB. The mechanism can be described as a two-stage process, as schematically shown in Fig. 7. In the first stage, a 60° unit dislocation with the Burgers vector of $D'B$ (1/2 [0 1 1]) on AD′B (−1 −1 1) plane encountered the TB on ABC (1 1 1) plane, and then dissociates into a Frank partial dislocation $D'\delta$ (1/3[1 1 1]) and a Shockley partial dislocation δB (1/6[−2 1 1]). The above interaction is expressed as:

$$D'B \rightarrow D'\delta + \delta B \tag{2}$$

The interaction energy ΔE_1 [27] in the first stage is expressed as:

$$\Delta E_1 = E_{D'\delta} + E_{\delta B} + E_{D'\delta-\delta B} - E_{D'B} = 2.5 \times \left[\frac{Ga^2}{72\pi(1-\upsilon)}\right]$$

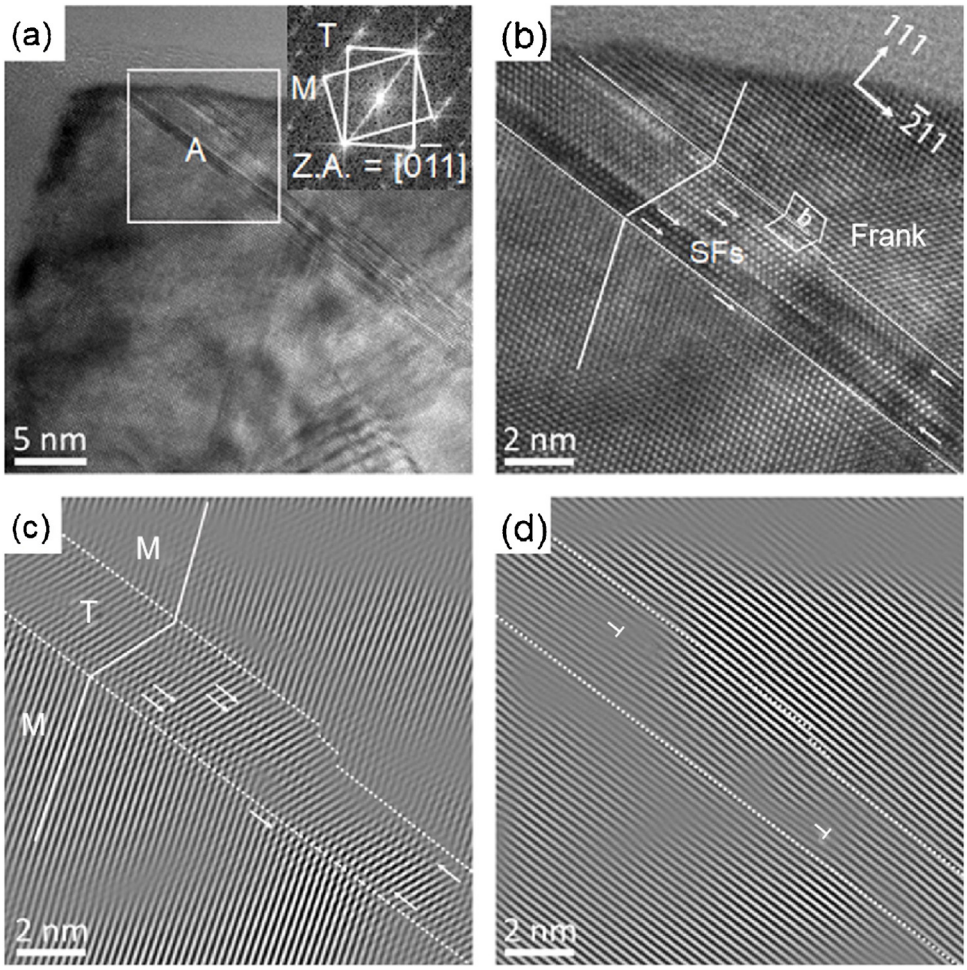

Fig. 3 – (a) [0 –1 1] zone axis (Z.A.) HRTEM image of the HPT processed Cu-30% Zn alloy. FFT pattern of inset revealed a twin relationship. (b) High magnification image of region A in (a), showing a twin lamella (marked as "T") interspersed in the matrix ("M"), SFs (marked by white arrows) and dislocations (marked by white "⊥") in the twin lamella. Frank circuit is conducted around the TB steps. (c, d) Corresponding $(-1\,1\,1)_{M/T}$ and $(1\,1\,1)_{M/T}$ inverse filtered Fourier transformation (IFFT) images of (b) to analyze SFs and dislocations.

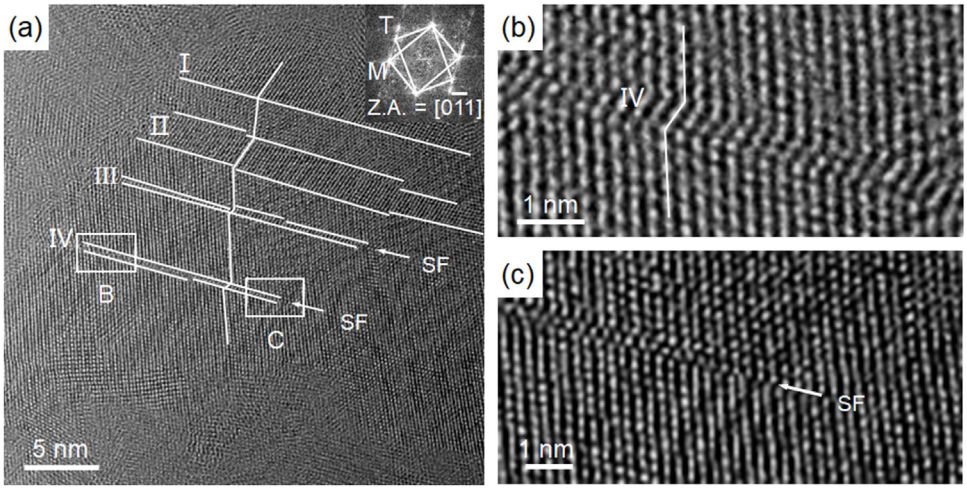

Fig. 4 – (a) [0 –1 1] zone axis (Z.A.) HRTEM image of the HPT processed Cu-30% Zn alloy showing four twin lamellae (marked as I, II, III and IV), and SFs (marked by white arrows). (b, c) High magnification images of regions B and C in (a).

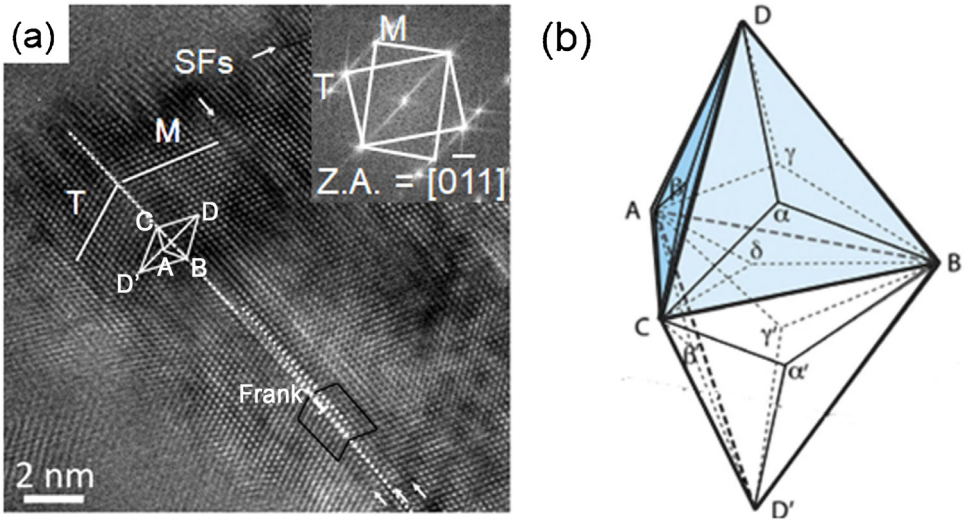

Fig. 5 – (a) [0 –1 1] zone axis (Z.A.) HRTEM image the HPT processed Cu-30% Zn alloy displaying a TB with one (1 1 1) atomic layer. Twin lamella and matrix are marked as "T" and "M" respectively. Frank circuit and double Thompson tetrahedron were conducted on the TB with a step. (b) Schematic illustration of double Thompson tetrahedron. The top Thompson tetrahedron above the ABC (1 1 1) TB represents matrix slip systems, while the bottom tetrahedron represents twin slip systems [44].

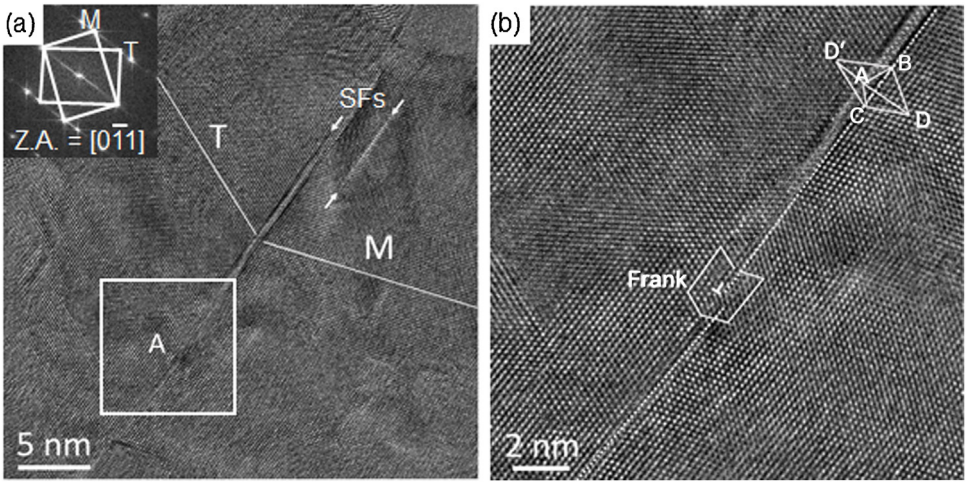

Fig. 6 – (a) A [0 –1 1] zone axis (Z.A.) HRTEM image of the HPT processed Cu-30% Zn alloy, showing twin (marked as "T") and SFs (marked by white arrows). (b) High magnification image of the region A in (a). Frank circuit and double Thompson tetrahedron is conducted on the TB. TB step with multiple (1 1 1) layers is found.

$$-4.24\times\left[\frac{Ga^2}{72\pi(1-\upsilon)}\right]\times\ln\left(\frac{R}{\bar{d}}\right) \tag{3}$$

where $E_{D'\delta}$, $E_{\delta B}$ and $E_{D'B}$ are the energies of $D'\delta$, δB and $D'B$ respectively; $E_{D'\delta-\delta B}$ is the separation energy between the partial dislocations of $D'\delta$ and δB, G is the shear modulus, υ is the Poisson's ratio, a is the lattice constant, and R is the spacing between the partial dislocations of $D'\delta$ and δB. MD simulation [12] revealed that the above reaction is an energy decreasing process, hinting the feasibility of the unit dislocation dissociation driven by the external stress in the FCC structured Cu-30% Zn alloy. According to the above analysis in Fig. 6, the dissociation of the unit dislocation formed a one atomic layer step on the TB by the slip of the Shockley partial dislocation δB along the TB.

The second stage is a process of the dislocation emission from the TB with step. Once the Shockley partial dislocation δB slips away, the Frank partial $D'\delta$ (1/3[1 1 1]) dissociates into a unit dislocation $D'B$ (1/2[0 1 1]) and a Shockley partial dislocation $B\delta$ (1/6[2 –1 –1]), as shown in the Fig. 7c. The above interaction is expressed as:

$$D'\delta \rightarrow D'B + B\delta \tag{4}$$

For the dissociation, elastic energy change is irrelevant because the reaction separates by one atomic layer and occurs

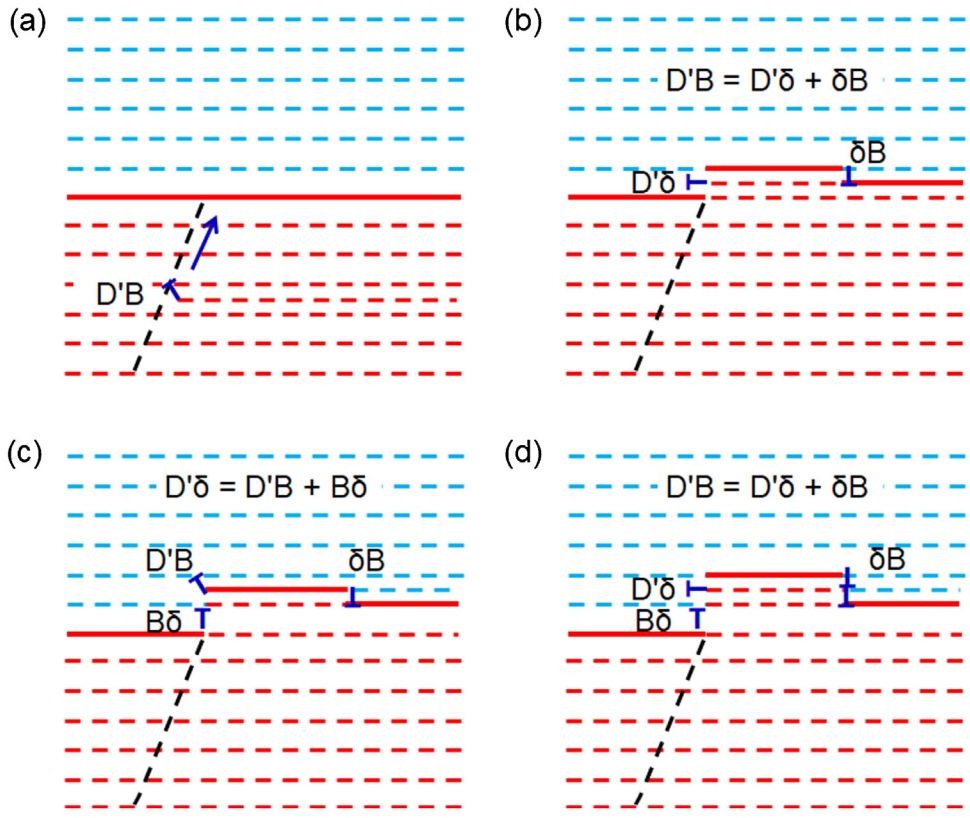

Fig. 7 – (a–d) Schematic illustration of the migration mechanism of TB through the interaction of a unit dislocation *D′B* with the TB [27].

over core dimensions. Li et al. [27] suggested two factors promotes the interaction: (i) the dislocation core relaxes, and (ii) the newly generated unit dislocation continue slip transmission. As shown in the Fig. 7d, the unit dislocation *D′B* (1/2[0 1 1]) once again dissociated under the external shear stress by the reaction equation in the first stage. Therefore, the repeated interaction caused the TB with multiple atomic layers step.

The interaction energy ΔE_2 [27] in the second stage is expressed as:

$$\Delta E_2 = E_{D'\delta} + 2E_{\delta B} + E_{B\delta} + E_{D'\delta-B\delta-2\delta B} - (E_{D'\delta} + E_{\delta B} + E_{D'\delta-\delta B})$$

$$= 4.5 \times \left[\frac{Ga^2}{72\pi(1-\upsilon)}\right] \times \ln\left(\frac{\sqrt{2}d}{a}\right) + 6.2 \times \left[\frac{Ga^2}{72\pi(1-\upsilon)}\right] - 13.24 \times \left[\frac{Ga^2}{72\pi(1-\upsilon)}\right] \times \ln\left(\frac{R}{d}\right) \quad (5)$$

where the $4.5 \times \left[\frac{Ga^2}{72\pi(1-\upsilon)}\right] \times \ln\left(\frac{\sqrt{2}d}{a}\right) + 6.2 \times \left[\frac{Ga^2}{72\pi(1-\upsilon)}\right]$ is the energy variation of the multiplication process, and the $13.24 \times \left[\frac{Ga^2}{72\pi(1-\upsilon)}\right] \times \ln\left(\frac{R}{d}\right)$ is the interaction energy, which significantly reduces the whole reaction energy. The MD simulation conducted in a Cu cell with a Frank dislocation and an associated step supports the above proposed model [27].

Except the above proposed model, Zhu et al. [55] reported another mechanism of the interaction between the incoming 60° unit dislocation and the TB. First, *D′B* encounter the TB, and dissociate according to Eq. (2). In the double Thompson tetrahedron, $D'\delta$ is equivalent to δD, which can further dissociate and emit unit dislocations at TB according to:

$$D'\delta = \delta D \rightarrow \delta B + BD \quad (6)$$

$$D'\delta = \delta D \rightarrow \delta C + CD \quad (7)$$

$$D'\delta = \delta D \rightarrow \delta A + AD \quad (8)$$

By substituting Eqs. (6)–(8) into Eq. (2), and also considering $\delta C + \delta B = A\delta$ and $\delta C + \delta A = B\delta$, the following reaction equations are obtained:

$$D'B \rightarrow 2\delta B + BD \quad (9)$$

$$D'B \rightarrow A\delta + CD \quad (10)$$

$$D'B \rightarrow C\delta + AD \quad (11)$$

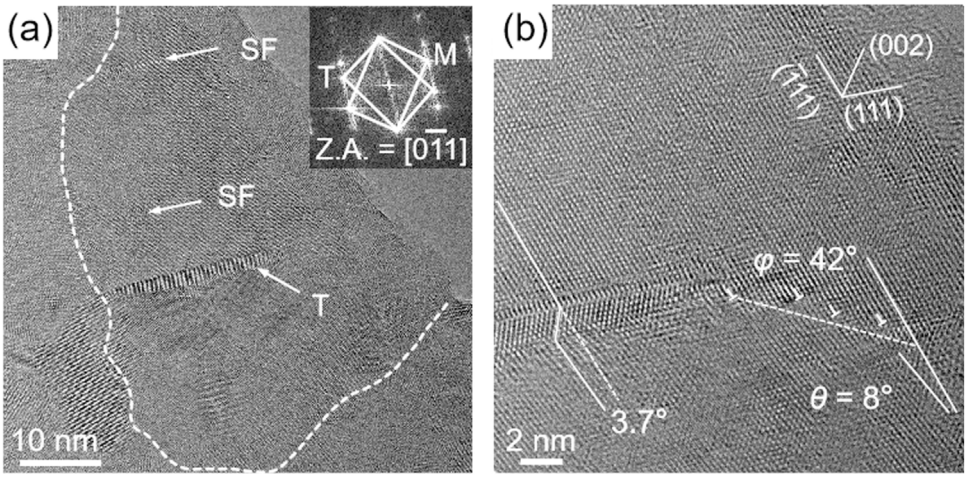

Fig. 8 – (a) [0 –1 1] zone axis (Z.A.) HRTEM image of the HPT processed Cu-30%Zn alloy showing the GB (marked by white dotted line), SFs (marked by white arrows) and the twin lamella (marked as "T"). (b) High magnification image in (a) showing the accumulation of dislocations pinned the twin propagation and formed an asymmetric tilt GB.

The energy barriers ΔE_3, ΔE_4 and ΔE_5 for the above dislocation reactions in Eqs. (9)–(11) expressed as [54]:

$$\Delta E_3 \approx \frac{Ga^2(1-3\upsilon/4)}{12\pi(1-\upsilon)}\ln\frac{\sqrt{2}d}{a}+\frac{5Ga^2}{48\pi(1-\upsilon)} \tag{12}$$

$$\Delta E_4=\Delta E_5 \approx \frac{Ga^2}{24\pi(1-\upsilon)}\ln\frac{\sqrt{2}d}{a}+\frac{13Ga^2}{240\pi(1-\upsilon)} \tag{13}$$

So the dislocation reactions in Eqs. (10) and (11) have smaller energy barriers than that in Eq. (9). In these two reactions, one partial dislocation ($A\delta$ or $C\delta$) glides on the TB ABC (1 1 1) plane, leading to de-twinning/twinning and leaving an atomic step on TB. At the same time, the interaction induces a 60° unit dislocation in the matrix and produces an atomic step on the TB. While two partials two partials (δB) are released on (1 1 1) TB plane via the interaction in the Eq. (9), leading to twin grow/shrinkage of two atomic planes.

3.4. *Strengthening mechanism of pinned twin lamella*

Except the above interactions between dislocations and TBs, the propagation of twin lamellae prevented by the dislocations pinning was also observed, as shown in Fig. 8. A 80 nm sized grain (GB marked by white dotted line) was found to have two SFs (marked by two white arrows) and a deformation twin with a thickness of 2 nm (Fig. 8a). The deformation twin, nucleated at the left GB, propagated towards right side, but terminated in the grain interior. The high magnification image in Fig. 8b shows that there are four unit dislocations (marked by white "⊥") pinned at the end of the twin and block the twin propagation. Moreover, the four dislocations induced an asymmetric tilt GB in matrix with a tilt angle φ, equal to 42°, and a misorientation of 8° in the matrix as well as a 3.7° misorientation between the (−1 1 1) planes above and below the twin. According to the classical dislocation model of asymmetric tilt GB in a cubic crystal [35], the average dislocation spacing D of perfect dislocation is expressed as:

$$D=\frac{b}{\cos(\varphi-\theta/2)-\cos(\varphi+\theta/2)} \tag{14}$$

where b is the Burgers vector of unit dislocations, θ is the misorientation. D is calculated as 2.79 nm, greater than the measured value of 1.74 nm in Fig. 8b, indicating the lattice distortion caused by the dislocation accumulation in the matrix is bigger than the theoretical value.

4. Conclusions

In this study, we prepared nanocrystalline Cu-30% Zn alloy with an average size of 80 nm by HPT and characterized the GB structures and TB-dislocation interactions revealed TB migration mechanisms. The main conclusions are as follows:

1. The severe plastic deformation produced curved GBs with nanoscale amorphous domain and non-equilibrium GBs containing massive dislocations.
2. The HRTEM analyses revealed that the TB with one or multiple (1 1 1) layer facets were formed either by the slip of Shockley partial dislocation along the TB, or by reversible reaction between a unit dislocation and the TB with the help of the dissociation of a sessile Frank partial dislocation.
3. The dislocation accumulation on the end of the twin lamella prevented its propagation, and formed an asymmetric tilt GB in matrix.

Conflict of interest

The authors declare no conflict of interest.

Acknowledgements

Y.H. Zhao acknowledges financial supports from National Key R&D Program of China (Grant No. 2017YFA0204403) and the National Natural Science Foundation of China (Grant Nos. 51971112 and 51225102) as well as the Fundamental Research Funds for the Central Universities (Grant No. 30919011405).

REFERENCES

[1] Ovid'ko IA, Valiev RZ, Zhu YT. Review on superior strength and enhanced ductility of metallic nanomaterials. Prog Mater Sci 2018;94:462–540.
[2] Zhao YH, Zhu YT, Lavernia EJ. Strategies for improving tensile ductility of bulk nanostructured materials. Adv Eng Mater 2010;12:769–78.
[3] Horita Z, Ohashi K, Fujita T, Kaneko K, Langdon TG. Achieving high strength and high ductility in precipitation-hardened alloys. Adv Mater 2005;17:1599–602.
[4] Zhao YH, Liao XZ, Cheng S, Ma E, Zhu YT. Simultaneously increasing the ductility and strength of nanostructured alloys. Adv Mater 2006;17:2280–3.
[5] Wu X, Yang M, Yuan F, Wu G, Wei Y, Huang X, et al. Heterogeneous lamella structure unites ultrafine-grain strength with coarse-grain ductility. PNAS 2015;112:14501–5.
[6] Wang Y, Chen M, Zhou F, Ma E. High tensile ductility in a nanostructured metal. Nature 2002;419:912–4.
[7] Zhao YH, Liao XZ, Horita Z, Langdon TG, Zhu YT. Determining the optimal stacking fault energy for achieving high ductility in ultrafine-grained Cu-Zn alloys. Mater Sci Eng A 2008;493:123–9.
[8] Lu L, Shen YF, Chen XH, Qian LH, Lu K. Ultrahigh strength and high electrical conductivity in copper. Science 2004;304:422–6.
[9] Lu K, Lu L, Suresh S. Strengthening materials by engineering coherent internal boundaries at the nanoscale. Science 2009;324:349–52.
[10] Lu L, Chen X, Huang X, Lu K. Revealing the maximum strength in nanotwinned copper. Science 2009;323:607–10.
[11] Zhao YH, Zhu YT, Liao XZ, Horita Z, Langdon TG. Tailoring stacking fault energy for high ductility and high strength in ultrafine grained Cu and its alloy. Appl Phys Lett 2006;89:121906.
[12] Li XY, Wei YJ, Lu L, Lu K, Gao HJ. Dislocation nucleation governed softening and maximum strength in nano-twinned metals. Nature 2010;464:877–80.
[13] Zhu L, Ruan H, Li X, Dao M, Gao H, Ju J. Modeling grain size dependent optimal twin spacing for achieving ultimate high strength and related high ductility in nanotwinned metals. Acta Mater 2011;59:5544–57.
[14] You ZS, Li XY, Gui LJ, Lu QH, Zhu T, Gao HJ, et al. Plastic anisotropy and associated deformation mechanisms in nanotwinned metals. Acta Mater 2003;61:217–27.
[15] You ZS, Lu L, Lu K. Tensile behavior of columnar grained Cu with preferentially oriented nanoscale twins. Acta Mater 2011;59:6927–37.
[16] Zhu T, Gao H. Plastic deformation mechanism in nanotwinned metals: an insight from molecular dynamic and mechanistic modeling. Scr Mater 2012;66:843–8.
[17] Wang YM, Sansoz F, LaGrange T, Ott RT, Marian J, Barbee JTW, et al. Defective twin boundaries in nanotwinned metals. Nat Mater 2013;12:697–702.
[18] Chassagne M, Legros M, Rodney D. Atomic-scale simulation of screw dislocation/coherent twin boundary interaction in Al, Au, Cu and Ni. Acta Mater 2011;59:1456–63.
[19] Lu N, Du K, Lu L, Ye HQ. Transition of dislocation nucleation induced by local stress concentration in nanotwinned copper. Nat Commun 2015;6:7648.
[20] Jin ZH, Gumbsch P, Albe K, Ma E, Lu K, Gleiter H, et al. Interactions between non-screw lattice dislocations and coherent twin boundaries in face-centered cubic metals. Acta Mater 2008;56:1126–35.
[21] Jin ZH, Gumbsch P, Ma E, Albe K, Lu K, Hahn H, et al. The interaction mechanism of screw dislocation with coherent twin boundaries in different face-centred cubic metals. Scr Mater 2006;54:1163–8.
[22] Gu P, Dao M, Suresh S. Analysis of size-dependent slip transfer and inter-twin flow stress in a nanotwinned fcc metal. Acta Mater 2014;67:409–17.
[23] Wu ZX, Zhang YW, Strolovitz DJ. Deformation mechanisms, length scales and optimizing the mechanical properties of nanotwinned metals. Acta Mater 2011;59:6890–900.
[24] Zhou H, Li X, Qu S, Yang W, Gao H. A jogged dislocation governed strengthening mechanism in nanotwinned metals. Nano Lett 2014;14:5075–80.
[25] Lu QH, You ZS, Huang XX, Hansen N, Lu L. Dependence of dislocation structure on orientation and slip systems in highly oriented nanotwinned Cu. Acta Mater 2017;127:85–97.
[26] Wang J, Li N, Anderoglu O, Zhang X, Misra A, Huang JY, et al. Detwinning mechanisms for growth twins in face-centered cubic metals. Acta Mater 2010;58:2262–70.
[27] Li N, Wang J, Misra A, Zhang X, Huang JY, Hirth JP. Twinning dislocation multiplication at a coherent twin boundary. Acta Mater 2011;59:5989–96.
[28] An XH, Song M, Huang Y, Liao XZ, Ringer SP, Langdon TG, et al. Twinning via the motion of incoherent twin boundaries nucleated at grain boundaries in a nanocrystalline Cu alloy. Scr Mater 2014;72–73:35–8.
[29] Cao Y, Wang YB, An XH, Liao XZ, Kawasaki M, Ringer SP, et al. Grain boundary formation by remnant dislocations from the de-twinning of thin nano-twin. Scr Mater 2015;100:98–101.
[30] Yamakov V, Wolf D, Phillpot SR, Gleiter H. Dislocation-dislocation and dislocation-twin reactions in nanocrystalline Al by molecular dynamic simulation. Acta Mater 2003;51:4135–47.
[31] Li YS, Dai LJ, Cao Y, Zhao YH, Zhu YT. Grain size effect on deformation twin thickness in ananocrystalline metal with low stacking-fault energy. J Mater Res 2019;194: 2398–405.
[32] Schioz J, Jacobsen KW. A maximum in the strength of nanocrystalline copper. Nature 2003;301:1357–9.
[33] Yamakov V, Wolf D, Phillpot SR, Mukherjee AK, Gleiter H. Deformation-mechanism map for nanocrystalline metals by molecular-dynamics simulation. Nat Mater 2004;3:43–7.
[34] Gutkin MY, Ovid'ko IA, Skiba NV. Crossover from grain boundary sliding to rotational deformation in nanocrystalline materials. Acta Mater 2003;51:4059–71.
[35] Shan ZW, Stach EA, Wiezorek JMK, Knapp JA, Follstaedt DM, Mao SX. Grain boundary-mediated plasticity in nanocrystalline nickel. Science 2004;305:654–7.
[36] Cheng S, Zhao YH, Guo Y, Li Y, Wei Q, Wang XL, et al. High plasticity and substantial deformation in nanocrystalline NiFe alloys under dynamic loading. Adv Mater 2009;21:5001–4.
[37] Wang YB, Li BQ, Sui ML, Mao SX. Deformation-induced grain rotation and growth in nanocrystalline Ni. Appl Phys Lett 2008;92:011903.
[38] Rupert TJ, Gianola DS, Gan Y, Hemker KJ. Experimental observations of stress-driven grain boundary migration. Science 2009;326:1686–90.
[39] Legros M, Gianola DS, Hemker KJ. In situ TEM observations of fast grain-boundary motion in stressed nanocrystalline aluminum films. Acta Mater 2008;56:3380–93.

[40] Kumar KS, Suresh S, Chisholm MF, Horton JA, Wang P. Deformation of electrodeposited nanocrystalline nickel. Acta Mater 2003;51:387–405.
[41] Moldovan D, Wolf D, Phillpot SR. Theory of diffusion-accommodated grain rotation in columnar polycrystalline microstructures. Acta Mater 2001;49:3521–32.
[42] Wang JW, Narayanan S, Huang JY, Zhang Z, Zhu T, Mao SX. Atomic-scale dynamic process of deformation-induced stacking fault tetrahedra in gold nanocrystals. Nat Commun 2013;4:2340.
[43] Liao XZ, Zhou F, Lavernia EJ, Srinivasan SG, Baskes MI, He DW, et al. Deformation mechanism in nanocrystalline Al: partial dislocation slip. Appl Phys Lett 2003;83:632–4.
[44] Zhu YT, Liao XZ, Wu XL. Deformation twinning in nanocrystalline materials. Prog Mater Sci 2012;57:1–62.
[45] Wang YB, Liao XZ, Zhao YH, Lavernia EJ, Ringer SP, Horita Z, et al. The role of stacking faults and twin boundaries in gain refinement of a Cu-Zn alloy processed by high-pressure torsion. Mater Sci Eng A 2010;527:4959–66.
[46] Ovid'ko IA, Reizis AB. Effect of elastic distortions on solid-state amorphization at grain boundaries and dislocations. J Phys D Appl Phys 1999;32:2833.
[47] Lkeda H, Qi Y, Cagin T, Samwer K, Johnson WL, Goddard WA. Strain rate induced amorphization in metallic nanowires. Phys Rev Lett 1999;82:2900.
[48] Li M. Defect-induced topological order-to-disorder transition in two-dimensional binary substitutional solid solutions: A molecular dynamics study. Phys Rev B 2000;62:13979.
[49] Peterlechner M, Waitz T, Karnthaler HP. Nanoscale amorphization of severely deformed NiTi shape memory alloy. Scr Mater 2009;60:1137–40.
[50] Inaekyan K, Brailovski V, Prokoshkin S, Korotitskiy A, Glezer A. Characterization of amorphous and nanocrystalline Ti-Ni-basd shape memory alloys. J Alloys Compd 2009;473:71–8.
[51] Révész Á, Hóbor S, Lábár JL, Zhilyaev AP, Kovács Z. Partial amorphization of a Cu-Zr-Ti alloy by high pressure torsion. J Appl Phys 2006;100:103522.
[52] Wu X, Tao N, Hong Y, Lu J, Lu K. Localized solid-state amorphization at grain boundaries in a nanocrystalline Al solid solution subjected to surface mechanical attrition. J Phys D Appl Phys 2005;38:4140.
[53] Tang LL, Zhao YH, Liang NN, Islamgaliev RK, Valiev RZ, Zhu YT. Localized deformation via multiple twinning in a Mg-Gd-Y-Zr alloy processed by high-pressure torsion. Mater Sci Eng A 2016;677:68–75.
[54] Yu YN. Foundation of materials science. Higher Education Press; 2005. p. 423–4.
[55] Zhu YT, Wu XL, Liao XZ, Narayan J, Kecskés LJ, Mathaudhu SN. Dislocation-twin interactions in nanocrystalline fcc metals. Acta Mater 2011;59:812–21.
[56] Wang J, Anderoglu O, Hirth JP, Misra A, Zhang X. Dislocation structure of Σ3 {112} twin boundaries in face centered cubic metals. Appl Phys Lett 2009;95:021908.
[57] Wang J, Misra A, Hirth JP. Shear response of Σ3 {112} twin boundary in face-centered cubic metals. Phys Rev B 2011;83:064106.
[58] Liu L, Wang J, Gong SK, Mao SX. High resolution transmission electron microscopy observation of zero-strain deformation twinning mechanisms in Ag. Phys Rev Lett 2011;106:175504.
[59] Zhang XY, Wu XL, Zhu AW. Growth of deformation twins in room-temperature rolled nanocrystalline nickel. Appl Phys Lett 2009;94:121907.
[60] An XH, Lin QY, Wu SD, Zhang ZF. Mechanically driven annealing twinning induced by cyclic deformation in nanocrystalline Cu. Scr Mater 2013;68:988–91.